Characteristics of High-Ion-Temperature Plasmas heated by Neutral Beams in the Large Helical Device

K. Nagaoka[1)], M. Yokoyama[1)], Y. Takeiri[1)], K. Ida[1)], M. Yoshinuma[1)], S. Matsuoka[2)], S. Morita[1)], K. Tanaka[1)], H. Funaba[1)], K. Ikeda[1)], M. Osakabe[1)], T. Mutoh[1)], T. Seki[1)], K. Tsumori[1)], Y. Oka[1)], O. Kaneko[1)] and LHD experimental group

1) National Institute for Fusion Science, Toki 509-5292, Japan
2) The Graduate University for Advanced Studies, Toki 509-5292, Japan

e-mail : nagaoka@LHD.nfis.ac.jp

Abstract. Improvement of ion heat transport in Heliotron plasmas has been realized by upgrade of ion heating power by using low energy neutral beam (NB) in the Large Helical Device (LHD). Ion internal transport barrier (ITB) (the peaked profile of ion temperature (T_i) with steep gradient in the core region) has been formed and the central T_i of 6.8 keV has been achieved in hydrogen plasma with the line-averaged electron density of $2x10^{19}$ m^{-3}. The experimental ion thermal diffusivity significantly decreases to the neoclassical level, indicating significant reduction of anomalous transport. The analysis of neoclassical ambipolar diffusion showed the enhancement of the negative radial electric field (E_r<0) associated with the T_i increase, indicating that the anomalous transport is suppressed by the negative E_r. The ion transport inside the ITB shows negative dependence on the T_i and heating power, while that outside of ITB shows gyro-Bohm properties.

1. Introduction

Improved confinement is a key issue for thermonuclear fusion experiment in stellarators as well as in tokamaks. Internal improved modes have been realized in stellarators utilizing center-focused intense electron cyclotron heating (ECH), for example, electron internal transport barrier (ITB) in the Compact Helical System (CHS) [1], Wendelstein7-AS [2], TJ-II [3] and the Large Helical Device (LHD) [4-6], and the core electron temperature is significantly enhanced by the formation of these electron ITBs. The transition of radial electric field (E_r) from negative to positive was observed in the formation of electron ITB and the bifurcation of neoclassical (NC) E_r is considered as a mechanism of transition to electron ITB in stellarators [7]. On the other hand, ion confinement has not been progressed in comparison with electron confinement. In LHD, a production of high ion temperature (T_i) plasmas has been performed in high-Z plasmas [8]. The main heating tool in LHD is negative-ion-based neutral beam injections (N-NBIs) with the high beam energy of 180 keV, which mainly heat electrons due to much higher beam energy than the critical energy. In order to increase the ion heating power, high-Z plasmas have been produced by neon / argon gas puffing, and the central T_i of 13.5 keV was achieved in an argon plasma in LHD [8,9].
Recently, a positive-ion-based neutral beam injection (P-NBI) with relatively low beam energy was installed for ion heating and profile measurement of T_i and plasma rotations, and the ion confinement study has been significantly progressed in LHD [10,11]. In this paper, the main achievements of ion heating experiments in LHD are presented. The experimental setup is briefly mentioned in Sec. 2. The ion ITB formation and the extension of high-T_i regime of helical plasmas are presented in Sec. 3. The comparison of observed ion thermal diffusivity with NC transport and transport characteristics of ion ITB plasma are presented in Sec. 4. The impurity transport and toroidal rotation in associated with ion ITB are discussed in Sec. 5, and summarized in Sec. 6.

2. Experimental Setup

2.1. LHD

The experimental stage is the LHD which is the world's largest superconducting magnetic confinement device employing a heliotron concept [12]. The magnetic field of up to 3 T is provided steadily. The toroidal and poloidal periods are n = 10 and m = 2, respectively. The major and averaged minor radii are 3.9 m and 0.6 m, respectively. The current plasma heating capability is 21 MW of neutral beam injection (NBI), 2.9 MW of ion cyclotron range of frequency (ICRF) and 2.1 MW of ECH. Three N-NBIs produce hydrogen neutral beams with the beam energy of 180 kV and total port-through power of 15MW [13]. The N-NBIs are tangentially injected to LHD plasma (BL1:co, BL2:counter and BL3:co-direction), and the NB driven plasma current and the toroidal momentum input are provided for various types of plasma experiments by means of the combination of N-NBIs. The P-NBI with low energy of 40 keV was newly installed and started the beam injection with the port-through power of 3MW in 2005 for ion heating and plasma diagnostic. Based on the success of ion heating utilizing P-NBI, the port-through power of P-NBI was upgraded up to 7MW at 2006 for high power ion heating experiments.

2.2. Charge Exchange Spectroscopy System

The charge exchange spectroscopy (CXS) system is used for profile measurement of T_i, toroidal flow velocity (V_t), poloidal flow velocity (V_p) and carbon impurity (n_{im}) in neutral beam heated plasmas in LHD. The charge exchange line of fully ionized carbon is measured by two different lines of sight; poloidal and toroidal lines of sight. The extreme hollow profile of carbon impurity (impurity hole) is formed when the ion temperature become high in the core region. The integration effect along the poloidal line of sight is serious problem in high-T_i discharges because the radius of probe beam (P-NBI) is almost half of the minor radius in the plasma. Thus the poloidal velocity and the radial electric field of the high-T_i plasma can not be obtained by CXS system, so the toroidal line of sight is utilized in this experiment. Two CXS systems were installed in the toroidal line of sight. One has a high spatial resolution of 20mm in the minor radius. The other has only four channels in the minor radius, in which the several optical fibers were bundled to increase the carbon line intensity in order to increase the accuracy of measurement in the carbon impurity hole. The half power of the probe beam (P-NBI) is modulated for measurement of back ground signals.

3. Formation of Ion ITB

3.1. ITB Discharge

The productions of high-T_i plasmas with low Z_{eff} have been performed by high power NB heating in LHD with the inwardly-shifted configurations with 3.575m < R_{ax} < 3.7m. The inward shifted configuration has a good particle confinement and the outward shifted has a good MHD stability in LHD configuration. The typical wave form of high-T_i discharge is shown in Fig. 1(a). At the beginning of the shot, the target plasma was started by ECH heating and sequentially connected to the low power NB heating phase utilizing P-NBI alone (P-NBI phase). In the P-NBI phase, the T_i profile is broad and the central T_i is almost 1.5 keV, which is shown in Fig. 1(b). After superposition of N-NBIs, the central T_i significantly increases up to 5.5 keV with the line-averaged electron density of almost 2×10^{19} m^{-3} and the

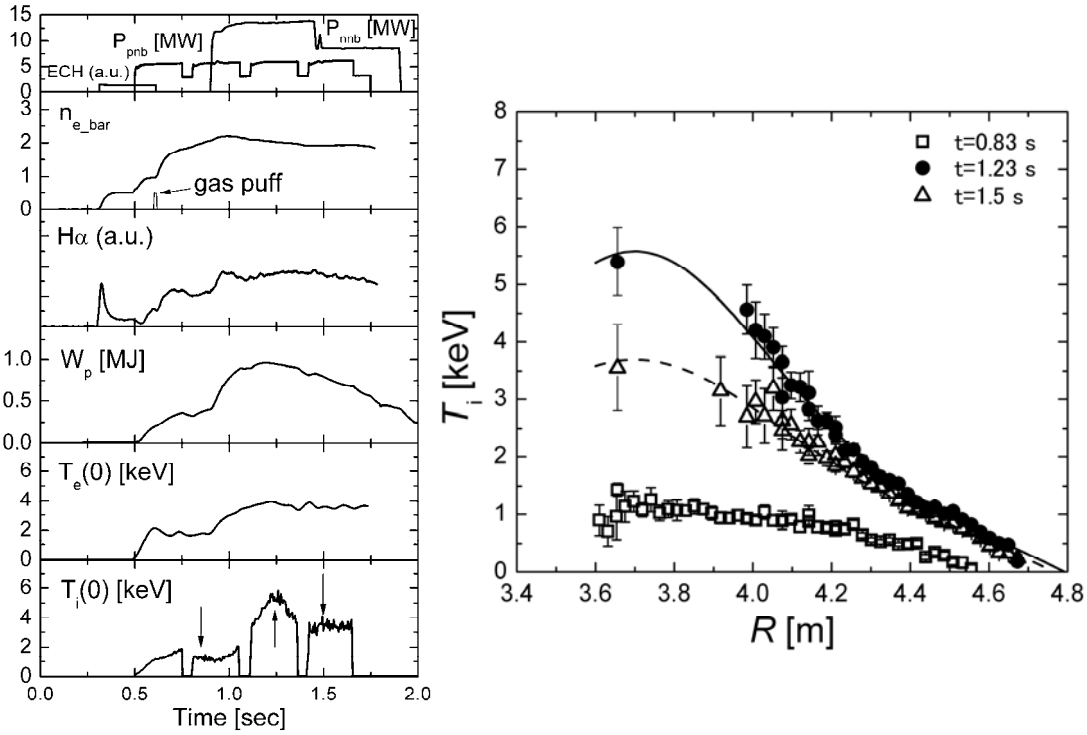

FIG. 1 (a) The typical wave form of high-T_i discharge in LHD (Shot No. 80268). The heating power of ECH, P-NBI and N-NBI are shown in the top. The time traces of the line averaged electron density, H_α emission, the stored energy, the central T_e and the central T_i are shown. (b) The T_i profiles in P-NBI phase (t = 0.83 s), the high T_i phase (t = 1.23 s) and no ITB phase (t = 1.5 s). These time slices are shown by arrows in the bottom graph of FIG. 1(a).

steep gradient is formed in the core region (ion ITB formation). The electron temperature also increases up to 4 keV, however the electron ITB is not formed simultaneously. The plasma with $T_i(0) > T_e(0)$ is produced in high-T_i phase. The high-T_i phase ($T_i > 0.8^* T_{i\_max}$) is maintained for 200 msec, which is almost several times longer than the energy confinement time.

3.2. Extension of High-T_i Regime

The density is controlled by hydrogen or helium gas puffing in P-NBI heating phase. The reason of utilizing helium gas puff is to keep low wall recycling condition, which is preferable for the increase of central T_i. The electron density was scanned, and the central T_i in the P-NBI phase and the ITB phase are shown in Fig. 2(a). The central T_i in low density regime (lower than 2×10^{19} m^{-3}) becomes high, and the central T_i of 6.8 keV was achieved with the line-averaged electron density of 2×10^{19} m^{-3}, which is a new record in stellarators. In high density regime, the central T_i slowly decreases with the density, and the central T_i of 2.9keV was achieved with the density of 3.7×10^{19} m^{-3}. It is noted that the high-T_i plasma was also extended to high density regime.

The maximum central T_i of each discharge is sensitive to direct ion heating power of the NBs as shown in Fig. 2(b). The power threshold is recognized as $(P_i/n_i)_{th} = 4.3 \times 10^{-19}$MWm^3, where n_i is ion density estimated by the assumption that the averaged Z_{eff} is 2. In the low power regime, the power dependence of $T_i(0) \propto \left(P_i / n_i\right)^{0.4}$ was obtained, which is shown by

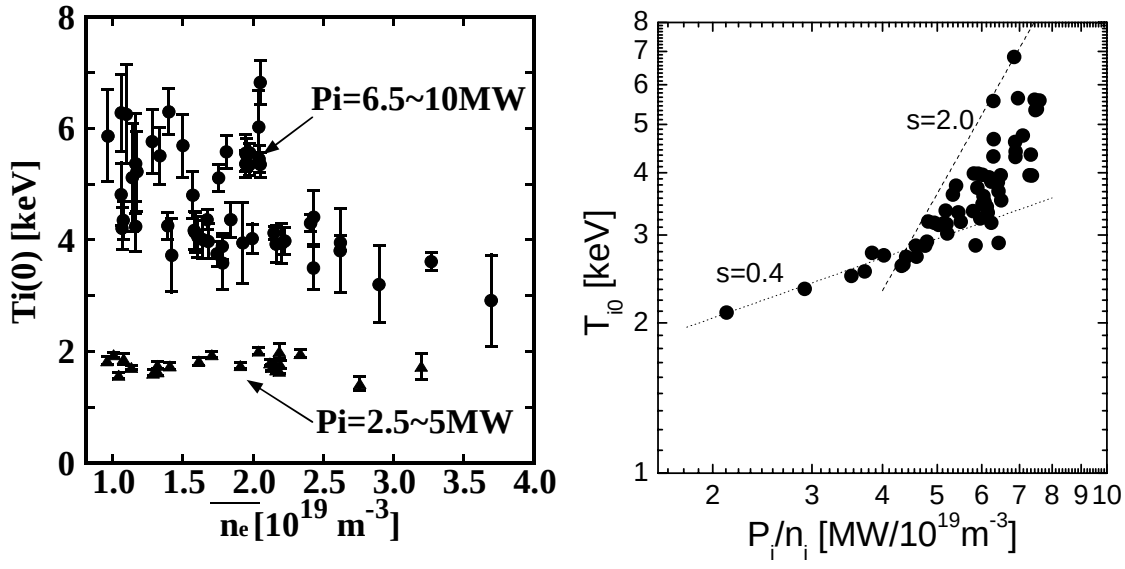

FIG. 2 (a) The maximum central T_i of each shot are shown by closed circles as a function of line-averaged electron density. The central T_i in P-NBI phase is also shown by closed triangles. (b) The maximum central T_i of each shot as a function of direct ion heating power of NBs normalized by ion density. The ion density is estimated by the assumption that the averaged Z_{eff} is 2. The power relations of $T_i(0) \propto \left(P_i / n_i\right)^{0.4}$ and $T_i(0) \propto \left(P_i / n_i\right)^{2.0}$ are shown by *dotted line and dashed line, respectively.*

dotted line in Fig. 2(b), and it is consistent with scaling law of ISS04 [14]. In the high power regime over the threshold, the central T_i has a stronger dependence with the power of 0.4~2.0, which indicates the improvement of confinement, that is, the formation of ITB.

In the case that the target plasma is heated by N-NBIs, the ion ITB is also formed after the superposition additional NB heating. However the enhancement of T_i is slightly lower, indicating that the increase of T_i in this discharge scenario is sensitive to other parameters such as density profile, fraction of T_i / T_e, and so on. In general property of N-NBIs heated plasmas in LHD, the T_e is higher than T_i and the profile of the electron density tend to be flat or hollow, while the plasmas heated by P-NBI alone has T_e comparable to T_i and relatively peaked density profile. Therefore it is considered that the peaked density profile is preferable and the fraction of T_i / T_e is also a candidate of key parameter for the production of high-T_i plasmas.

4. Transport Analyses

4.1. Comparison with Neoclassical Transport

The transport analysis was carried out for the typical high-T_i discharge, and the ion thermal diffusivities in P-NBI phase and the ITB phase were compared. The heating power of NBs was calculated by FIT code. The Z_{eff} = 2 and stationary state were assumed. The ion thermal diffusivity (χ_{i_EXP}) is high level in the core region of P-NBI phase (without ITB), and it significantly decreases in the core when the ITB was formed, which is shown in Fig 3(b). The neoclassical (NC) calculation was also carried out by GSRAKE code [15] utilizing the

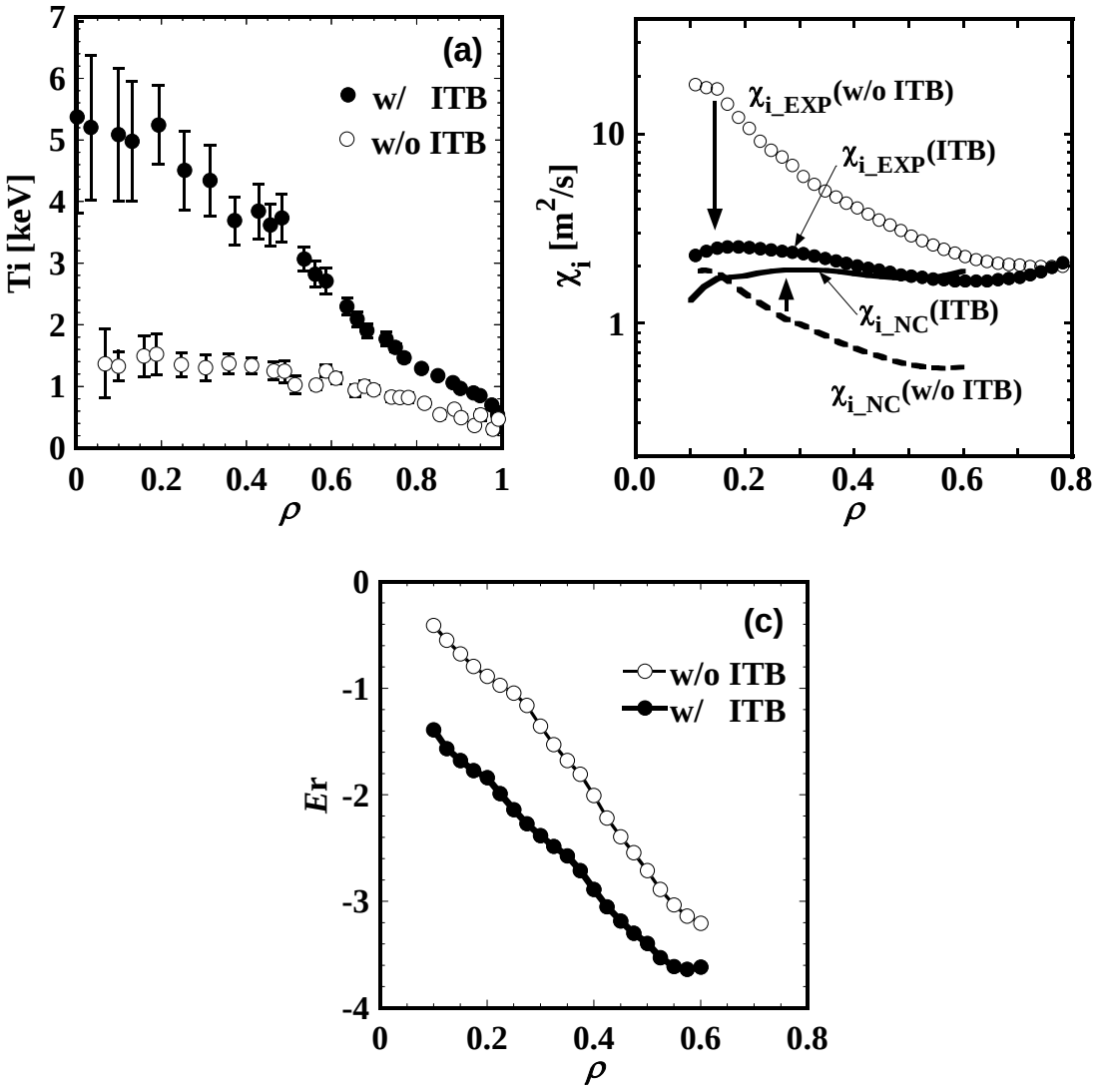

FIG. 3 (a) The T_i profiles at t = 0.75 sec in the P-NBI phase without ITB and at t = 1.15 sec in the ITB phase (Shot No. 74282). The direct ion heating powers in the P-NBI phase and in the ITB phase are 3 MW and 7 MW, respectively. (b) The experimental ion thermal diffusivities in the P-NBI phase and in the ITB phase and the NC ion diffusivities calculated by GSRAKE code are shown as a function of the normalized minor radius. (c) The radial electric fields in the P-NBI phase and in the ITB phase estimated based on the NC ambipolarity.

experimentally obtained density and temperature profiles. The NC ion thermal diffusivity (χ_{i_NC}) in P-NBI phase is almost 10^{-1} times lower than the experimental one (see Fig. 3(b)), thus the anomalous transport due to turbulence is dominant in P-NBI phase. On the other hand, the χ_{i_EXP}, is comparable to the χ_{i_NC} in ITB phase. Therefore, the turbulent transport is significantly reduced in the ITB phase. The radial electric field (E_r) was estimated based on the NC ambipolarity, which is shown in Fig. 3(c). Unfortunately, the E_r can not be experimentally observed in the ITB core region due to the formation of impurity hole. The NC E_r is a good indication of experimentally measured E_r in other experiments [16,17]. The E_r is negative (ion-root) in the whole region and becomes negatively large in the ITB phase, indicating that the reduction of anomalous transport is related to the enhancement of negative E_r in the ITB phase.

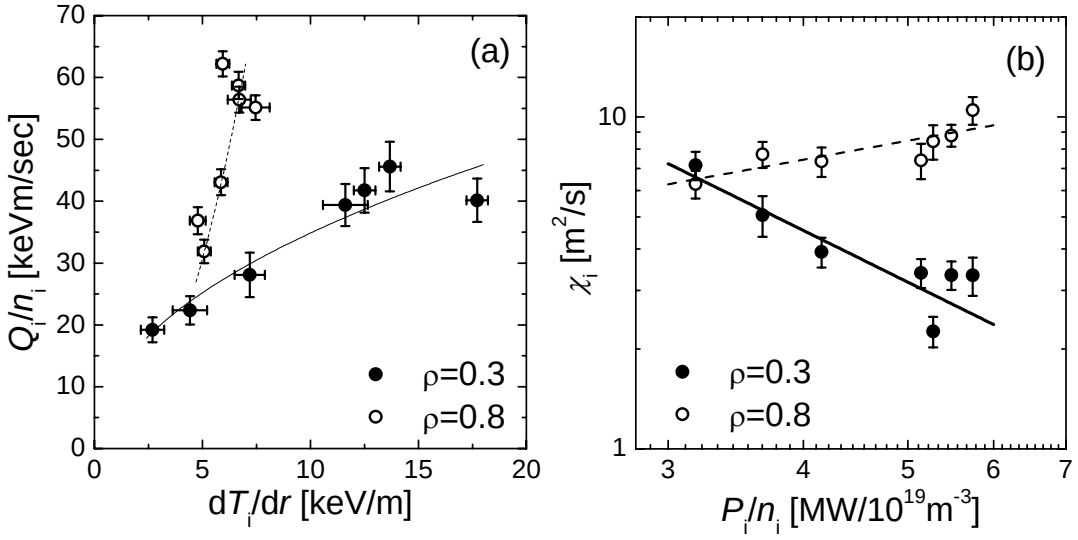

FIG. 4 (a) The ion heat fluxes at r = 0.3 (inside the ITB) and 0.8 (outside of the ITB) as a function of T_i gradient (Shot No.:80218, 80229, 80234, 80237, 80247, 80267, 80268). The dashed and solid lines show the dependence of $Q_i/n_i \propto T_i^{2.10}$ and $Q_i/n_i \propto T_i^{0.47}$, respectively, when $\partial T_i/\partial r \propto T_i$. *(b) The ion thermal diffusivity (χ_i) at r = 0.3 (inside the ITB) and 0.8 (outside of the ITB) as a function of direct ion heating power of NBs normalized by the ion density. The dashed and solid lines show the dependence of* $\chi_i \propto \left(P_i/n_i\right)^{0.59}$ *and* $\chi_i \propto \left(P_i/n_i\right)^{-1.61}$, *respectively .*

4.2. Transport Characteristics of ITB

In order to investigate the transport characteristics of ITB plasma, the several shots were analyzed in detail. The T_i profile in the core region was obtained by fitting the CXS data utilizing the fitting function of $T_i(\rho) = T_{i1} \cdot (\rho^2_{edge} - \rho^2) + T_{i2} \cdot \exp\left(-\rho^2 / w^2_{ITB}\right)$, where T_{i1}, T_{i2} and w_{ITB} are fitting parameters corresponding to the base T_i profile, ITB T_i profile and ITB width, respectively. The ρ_{edge} is the minor radius where T_i = 0. The Z_{eff} is assumed for simplicity as a hyperbolic tangent function to be 2 in the core and 3 in the periphery. The relation of ion heat flux to T_i gradient were compared between inside (ρ = 0.3) and outside (ρ = 0.8) of ITB foot as shown in Fig. 4(a). The ion heat flux in the outside of the ITB has a stronger dependence on the T_i gradient: $Q_i/n_i \propto T_i^{2.10}$ ($\chi_i \propto T_i^{1.10}$), which is shown by dashed line in Fig. 4(a). It is noted that the plasma outside of the ITB shows the gyro-Bohm dependence: $\left(Q_i/n_i\right)_{\text{gyro-Bohm}} \propto T_i^{5/2}$. On the other hand, the large T_i gradient is realized with smaller heat flux inside the ITB. The dependence of $Q_i/n_i \propto T_i^{0.47}$ ($\chi_i \propto T_i^{-0.53}$) is obtained, which is shown by dotted line in Fig. 4(a). The quite different dependences of χ_i on the direct ion heating power were observed between inside and outside of the ITB, and it is $\chi_i \propto \left(P_i/n_i\right)^{0.59}$ at outside of ITB and $\chi_i \propto \left(P_i/n_i\right)^{-1.61}$ inside of the ITB, which are shown in Fig. 4(b). The χ_i inside the ITB also shows the gyro-Bohm dependence: $\chi_{i\_\text{gyro-Bohm}} \propto \left(P_i/n_i\right)^{0.6}$. It is noted that the negative dependence of χ_i on the T_i: $\partial\chi_i/\partial T_i < 0$

and the heating power: $\partial\chi_i/\partial(P_i/n_i) < 0$ indicate the possibility of further confinement improvement due to increment of heating power in LHD.

5. Other Characteristics

5.1.Impurity Transport

In tokamaks, an impurity control is one of the issues to be solved associated with ITB formation, because impurities tend to accumulate in the core region due to negative E_r. In the ITB discharges of LHD, the carbon impurity significantly decreases in response to increase of T_i, and extremely hollow profile of impurity (impurity hole) is formed in the ITB phase, which is mainly reported by K. Ida et al. in EX/8-2Rb of this conference. The argon (Ar) impurity hole was also indicated by measurement of ArXVII line utilizing X-ray crystal spectrometer [18]. Although the E_r can not observed in the core of ITB plasma due to formation of impurity hole, the negative E_r is predicted by calculation of NC ambipolarity. Therefore the mechanism of formation of impurity hole can not be understood at this moment. The compatibility with ITB formation and impurity hole is a great advantage of ITB in helical plasmas, thus the understanding of property of impurity transport is a prime task.

5.2.Toroidal Rotation

Toroidal rotation is considered as an ITB control knob in reversed-shear configuration of tokamaks, and various type of toroidal rotation and the momentum transport have been investigated [19-21]. In LHD, an enhancement of toroidal rotation was observed in the core, when the ion ITB is formed. The direction of toroidal rotation in the ITB core is predominated by torque of tangentially injected NBIs. Thus the large toroidal rotation is considered as an NB driven flow. The gradient of toroidal rotation increases with T_i gradient, which indicates the strong coupling of ion thermal transport and ion momentum transport in the ITB plasma. The coupling is very interesting from view point of understanding the mechanism of anomalous transport reduction. An T_i gradient driven toroidal rotation and an E_r driven toroidal rotation were also identified in LHD [21], which is reported by M. Yoshinuma, et al. in EX/P5-1 of this conference.

6. Concluding Remarks

Due to significant increase of ion heating power using low-energy P-NBI, an ion ITB was formed in LHD plasmas heated by NBs and the central T_i of 6.8 keV was achieved with the line-averaged electron temperature of 2×10^{19} m^{-3}. The χ_{i_EXP} of the ITB plasma is decreases to χ_{i_NC} level, and the negative E_r (ion-root) is predicted in the whole plasma. The χ_i outside of ITB tends to have a gyro-Bohm properties, and the ion thermal transport of the ITB is characterized by the negative dependences of χ_i on T_i and heating power, that is, $\partial\chi_i/\partial T_i < 0$ and $\partial\chi_i/\partial(P_i/n_i) < 0$. These observations indicate the possibility of further confinement improvement with increment of heating power. On the other hand, it is not clear that the χ_i can be reduced much lower than χ_{i_NC}. Therefore The fraction of T_e / T_i is considered as a key parameter for further extension of high-T_i regime in helical configuration in order to suppress NC transport. The selective ion heating experiment using P-NBI with much higher power is planned in LHD. The impurity hole was observed in the core of ITB plasmas, where the negative E_r is predicted by calculation of NC ambipolarity, which is considered as a great

advantage of ITB in helical plasmas. The mechanism of compatibility with negative E_r and impurity hole formation can not be understood yet. The enhancement of toroidal rotation associated with the ITB was observed and attracts much attention from view point of connection of heat transport and momentum transport.

Acknowledgement

The authors greatly acknowledge all technical staff for excellent and reliable operation of LHD. One of the authors (K.N.) thanks Dr. Y. Kamada (JAEA) for fruitful comments and discussions. This work is supported by NIFS (NIFS06ULBB501).

References

[1] A. Fujisawa, H. Iguchi, T. Minami, et al., Phys. Rev. Lett. **82** (1999) 2669.
[2] H. Maassberg, C.D. Beidler, U. Gasparino, et al., Phys. Plasmas **7** (2000) 295.
[3] F. Castejón, V. Tribaldos, I. García-Cortés, et al., Nucl. Fusion **42** (2002) 271.
[4] K. Ida, T. Shimozuma, H. Funaba, et al., Phys Rev. Lett. **91** (2003) 085003.
[5] T. Shimozuma, S. Kubo, H. Idei, et al., Plasma Phys Control. Fusion **45** (2003) 1183.
[6] Y. Takeiri, T. Shimozuma, S. Kubo, et al., Phys. Plasmas **10** (2003) 1788.
[7] A. Fujisawa, Plasma Phys. Control. Fusion **44** (2002) A1.
[8] Y. Takeiri, S. Morita, K. Ikeda, et al., Nucl. Fusion **47** (2007) 1078.
[9] S. Morita, M. Goto, Y. Takairi, et al., Nucl. Fusion **43** (2003) 899.
[10] K. Nagaoka, M. Yokoyama, Y. Takeiri, et al., Plasma Fusion Res. **3** (2008) S1013.
[11] M. Yokoyama, K. Nagaoka, M. Yoshinuma, et al., Phys. Plasmas **15** (2008) 056111.
[12] O. Motojima, H. Yamada, A. Komori, et al., Nucl. Fusion **47** (2007) S668.
[13] O. Kaneko, Y. Takeiri, K. Tsumori, et al., Nucl. Fusion **43** (2003) 692.
[14] H. Yamada, J.H. Harris, A. Dinklage, et al., Nucl. Fusion **45** (2005) 1684.
[15] C.D. Beidler and W.D. D'haeseleer, Plasma Phys. Control. Fusion **37** (1995) 463.
[16] K. Ida, M. Yoshinuma, M. Yokoyama, et al., Nucl. Fusion **45** (2005) 391.
[17] M. Yokoyama, H. Maaβberg, C.D. Beidler, et al., Nucl. Fusion **47** (2007) 1213.
[18] S. Morita and M. Goto, Rev Sci. Instrm. **74** (2003) 2375.
[19] E.J. Doyle, W.A. Houlberg, Y. Kamada, et al., Nucl. Fusion **47** (2007) S18.
[20] M. Yoshida, Y. Kamada, H. Takenaga, et al., Plasma Fusion Res. **3** (2008) S1007.
[21] M. Yoshinuma, K. Ida, M. Yokoyama, K. Nagaoka, M. Osakabe and the LHD experimental Group, Plasma Fusion Res. **3** (2008) S1014.